Journal of Natural Gas Science and Engineering 77 (2020) 103231

Contents lists available at ScienceDirect

Journal of Natural Gas Science and Engineering

journal homepage: http://www.elsevier.com/locate/jngse

Pore structure characteristics and fractal dimension analysis of low rank coal in the Lower Indus Basin, SE Pakistan

Hassan Nasir Mangi [a,b,c], Yan Detian [a,b,*], Nayima Hameed [d], Umar Ashraf [e], Riaz Hussain Rajper [f]

[a] School of Earth Resources, China University of Geosciences, Wuhan 430074, PR China
[b] Key Laboratory of Tectonics and Petroleum Resources of Ministry of Education, China University of Geosciences, Wuhan 430074, PR China
[c] Geological Survey of Pakistan, Ministry of Energy, Karachi 75290, Sindh, Pakistan
[d] Halliburton Worldwide, Islamabad 44000, Pakistan
[e] College of Ecology and Environmental Sciences, Yunnan University (Chenggong Campus), Kunming 650500, PR China
[f] Center of Pure and Applied Geology, Sindh University of Jamshoro, 76080 Sindh, Pakistan

ARTICLE INFO

Keywords:
Coalbed methane
Pore structure
Fractal dimension
Lower Indus basin

ABSTRACT

The significance of pore structure and fractal characteristics is important for understanding untapped Coalbed Methane (CBM) exploration. In this study, these features of low rank coal in the lower Indus Basin, SE Pakistan, were evaluated using drill core samples from several locations. The pore size distribution and fractal dimension on adsorption (AdDs) and desorption (DeDs) values were systematically analyzed by scanning electron microscopy (SEM), low pressure adsorption N_2, and CO_2 methods for better evaluation of CBM and its pores geometrical mechanism. Coal petrographic properties, were investigated for macerals composition revealed a huminite domination. SEM analysis of various pore structures, showed first-developed pores present in the larger pores and thermogenic gas pores. CO_2 density functional theory revealed micropore particle size peaks in three adsorption phases on incremental pore volume (0.47–0.64 nm,0.64–0.83 nm, 0.83–11.11 nm), where gas molecules distort bonding with increasing pore size and define the micropore surface complexities. The mesopore size distribution analysis of differential and incremental pore areas indicated a transition zone at 22.8 nm, suggesting major micro-mesopores within smaller size particles. Nonhomogeneous particle sizes caused a dynamic range of peak trends due to different kinds of porespheres are interconnected with macrosphere, which can trap accessible and inaccessible gas molecules in the different pores structures. Fractal dimension analysis demonstrated that Ds values linear correlation showed a good fit for the AdDs value was 0.98–0.99, and 0.96 to 0.99 for the DeDs value. This finding showed that average obtained surface complexity of AdDs was 2.35, and the DeDs was 2.44 with notably more complicated pore roughness and high semifusinite content, possibly resulting in the higher DeDs value because larger pore spheres consist of microspheres.

1. Introduction

Coal is a complex, heterogeneous, organic rich sedimentary rock that can contain valuable methane resources. Its complex porous nature can have a significant impact on CBM generation and exploitation (Fu et al., 2017). The pore generation and evolution in coal can be affected by several internal and external factors (Owen et al., 2016; Zhang et al., 2017a). Internal factors include coal quality and maceral compositions (huminite/vitrinite, exinite, and inertinite), and external factors include metamorphism and surface water, which can cause moisture within the coal. The external factors govern pore architecture and impact adsorption processes occurs within the coal pore surface area, the diameter of the internal pore structure, the surface area, and the external surface area (Day et al., 2008; Qin et al., 2005). Coal metamorphism directly affects coal rank and huminite/vitrinite reflectance (R_o, max). It has been observed that different chemical and physical parameters within various coal ranks are greatly influenced by the U-shaped relationships and PSD within the coal (Yu, 1992), although several studies have revealed that the transition of micropores to transitional pores is the first stage of CBM accumulation (Bustin and Clarkson, 1998; Chen et al., 2018; Clarkson and Bustin, 1999).

Various criteria of fractal geometry has been applied to identify the

* Corresponding author. School of Earth Resources, China University of Geosciences, Wuhan 430074, PR China.
E-mail address: yandetian@cug.edu.cn (Y. Detian).

https://doi.org/10.1016/j.jngse.2020.103231
Received 25 October 2019; Received in revised form 23 February 2020; Accepted 25 February 2020
Available online 29 February 2020

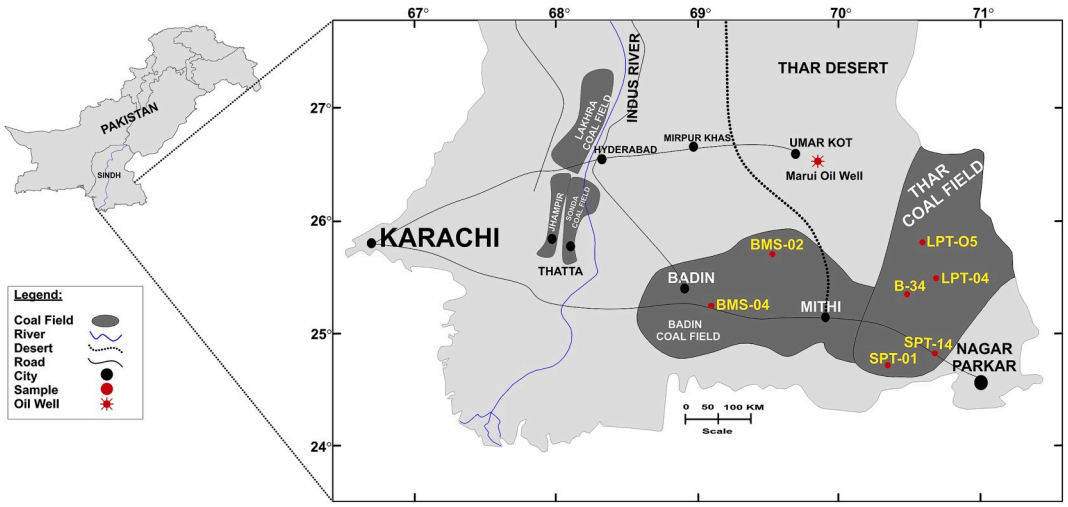

Fig. 1. Sample location map of the study areas: Thar and Badin, Sindh, Pakistan.

relationship between pore characteristics and surface irregularities within shale and coal. Fractal geometry was suggested by Mandelbrot (1975) to evaluate pore characteristics within porous media, such as coal (Li et al., 2016a,b,c; Sun et al., 2015). Bale and Schmidt (1984) performed Mandelbrot's experiment assessing fractal morphological structure on the Beulah lignite from North Dakota to investigate micropore structure. The surface fractal dimension was determined to have scattered curves in the lignite. Fractal dimension determinations have been performed on adsorption Ds values to assess pore surface complexities in recent studies (Li et al., 2016a,b,c; Sahouli et al., 1996; Yao et al., 2008), however, the relationship between pore surface and pore complexities continues to be debated.

Various advanced techniques can be used to document pore characteristics of coal qualitatively and quantitatively. These include scanning electron microscope (SEM), focused ion beam SEM (FIB-SEM), quantitative research N_2, and CO_2, nuclear magnetic resonance (NMR), mercury intrusion porosimetry (MIP), x-ray computed tomography (x-ray CT), small-angle x-ray scattering (SAXS), small-angle neutron scattering (SANS), and ultra-small angle neutron scattering (USANS) (Cui et al., 2009; Mastalerz et al., 2012). A coal surface area and pore size study relies on different techniques and methods for heterogeneous catalysis (Anovitz et al., 2015; Storck et al., 1998). With the quantitative microporosity analysis at low temperature and pressure, N_2 and CO_2 gas adsorption is more effective than qualitative method like SEM and transmission electron microscopy (TEM), as qualitative analysis alone is not a reliable method for analysis of organic matter (Anovitz et al., 2015; Clarkson et al., 2012; Mastalerz et al., 2017; Milliken et al., 2013). According to the International Union of Pure and Applied Chemistry (IUPAC) classifications, pores are categorized as micropores (<2-nm size), mesopores (2–50-nm), macropores (>50-nm), though previously Hodot (1960) classifications were used to quantify pore structure, pore volume, and pore distribution by MIP (Chen et al., 2018).

Two fundamental factors pore structure and gas adsorption significantly affect the CBM occurrence (Chen et al., 2018). Syngenetic gas originates during the coal diagenesis process, and the gas storage mechanism, at least in shallow depths. Lower-rank coals with the thickest coal seams are considered sufficient for CBM generation, as observed in the Powder River Basin, US (Boger et al., 2014). Therefore, for this study, the focus was on Thar coal's primary seam, which has thickness of 15–28.6 m with a 17.71 billion cubic meter reserve estimated to generate a three-dimensional (3D) seam volume model by ordinary kriging (Siddiqui et al., 2015).

Pakistan has indigenous natural fossil fuel resources, such as oil, gas, and coal. The cornerstone of unconventional resources (shale gas) and CBM have become significant energy resources with less carbon emission and are the first replacement of conventional resources (Mastalerz et al., 2017; Zhang et al., 2017b). In 1992, the US Geological Survey and the Geological Survey of Pakistan (GSP) jointly launched a CBM discovery program, and a TP-3 drilled hole was tested using primitive techniques to determine the presence of methane gas in the Thar coal block, Lower Indus Basin, SE Pakistan (SanFilipo, 2000). However, to improve the capitalization of untapped natural resources in this area a more advanced evaluation of the CBM is necessary.

To evaluate the fundamental pore characteristics for a basinal coal regime, we quantified the physiochemical coal relationship between micro- and macro-levels to create a regional level. To do so, it was necessary to evaluate pore morphological characteristics, a new kind of scientific investigation. Therefore, for the first time, we combined different types of technical investigations including coal assay, coal petrography, SEM, low temperature CO_2, and N_2 sorption, and fractal dimension in the Lower Indus Basin, specifically the Thar and Badin coal fields in Sindh, Pakistan. The coal pore structure and fractal dimension adsorption AdDs and desorption DeDs calculations were applied to evaluate this very promising coalbed methane resource area.

2. Geological setting

The Thar coal and Badin coalfield areas are located in the southeastern part of the Lower Indus Basin, Sindh, Pakistan (Fig. 1). The coal-bearing formation within the Lower Indus Basin is the Bara Formation, and Vredenburg (1909b) reported Lower Ranikot sandstone and additional categories within the Lower Ranikot (detrital sediments) and Upper Ranikot (carbonaceous sediments) (Vredenburg, 1909a). The Bara Formation is primarily composed of the following rock units: sandstone, siltstone, claystone, mudstone, shale, carbonaceous shale, carby clay, and coal.

Structurally, the Thar Plateform is situated in the southeastern part of Pakistan, over a Precambrian basement that has been described as the Nagarparkar Igneous Complex (NPIC). Tectonic events constrain compressional and extensional stresses caused by the emplacement of Nagarparkar Granite. The Thar coalfield lays on Precambrian rocks in a 9000 km^2 coal-bearing area (Fassett and Durrani, 1994), while the Badin coal-bearing horizons lay on Cretaceous rocks. Thar and Badin consist of mainly low rank coal-bearing horizons that are the same age as the Bara Formation. For this study, the focus was on the primary coal seam with an average thickness of 15–30 m, (Siddiqui et al., 2015). According to current drilling exploration data, Badin coal has thickness ranging from approximately 0.20 to 4 m, with an average thickness of 1–2 m.

The Thar platform shows a gentle 2 – 3° southwestward with variable basement trends and a horst and graben structural control at the Thar

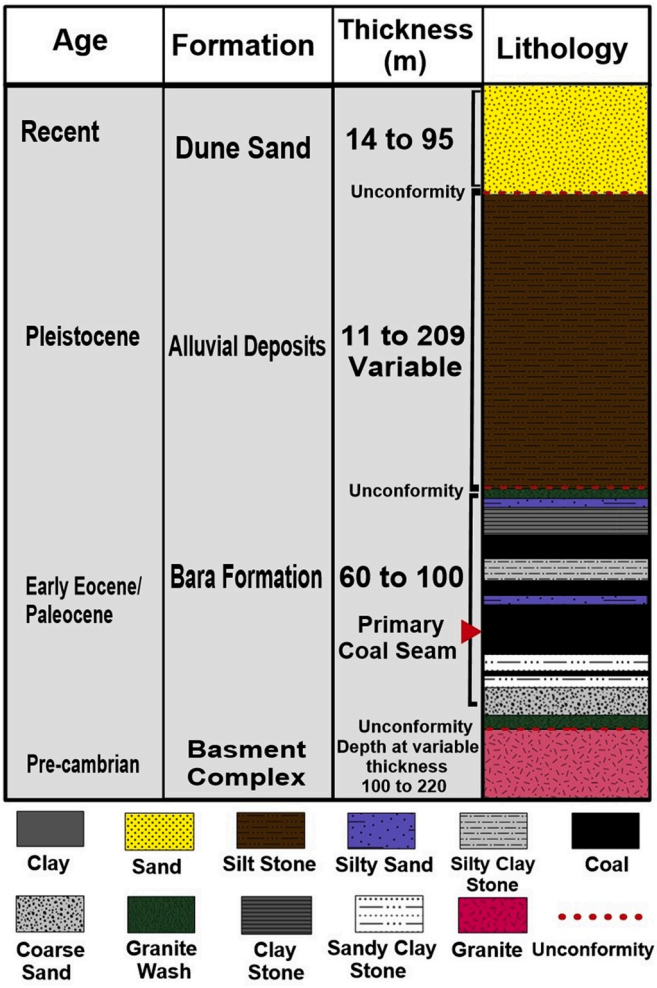

Fig. 2. Generalized stratigraphic column of the study area.

block. The Badin Block has deeper basement trends at >3000 m below sea level (Fassett and Durrani, 1994). The Nabisar oil exploration drill hole within the western part of the Thar coalfield and eastern part of the Badin Block and Marui oil well (located northwest of Thar and northeast of Badin Block) is close to previously mentioned blocks, indicating formation variation within the area. Top formations (i.e., Laki, Top Ghazij, and Ranikot Formation) at a depth of 411.48 m lay above the Bara Formation. The Thar and Badin Blocks indicate no sharp contact formation above the Bara Formation, which is covered by sub-recent to recent formations.

3. Materials and methods

3.1. Sampling method

Lignite samples were collected from Thar and Badin coal, the newly discovered coalfield blocks, and then 7 coal samples were randomly obtained from different bore -hole locations (Figs. 1 and 2). Five samples from Thar, SPT-01, SPT-14, B-34, LPT-04A, and LPT-05, and two samples from Badin Coalfield (BMS-02 and BMS-04) were selected. Care was taken during the preparation of each sample; samples were collected from the primary coal seam and top to bottom at a later time. A composite sample was prepared and packed into a polyethylene bag to contain moisture and to protect samples from impurities.

3.2. Coal analysis

For petrographic analysis the samples were pulverized to less than −1 mm, −18 mesh size, and coal pellets were prepared into the resin, mounted, and then polished. The petrographic analysis was performed on polished pellets using a Leitz Orthoplan Pol microscope, and Ro% reflective index was measured by a Leitz MPV-3 photometer, and microscope maceral counts were studied line by line and point to point on more than 500 counts performed. For the proximate test analysis, China National Standards GB/T 6948-2008 were followed. The final analysis was performed by CDRI Lucknow on a Vario EL III Element Analyzer following China National Standards GB/T 88992013. For qualitative analysis, the SEM method was applied on polished coal blocks, and selected samples were carbon-coated and analyzed for pore morphological characterization.

For pore geometry and fractal dimension analysis, the samples were pulverized and sieved at 0.18–0.25 mm, 60–80 mesh, and dried in a vacuum oven at 80 °C for 24 h to remove volatile substances and free water. Afterward, low pressure adsorption analyses were conducted on an ASAP 2020 for micropore characterization on low pressure CO_2 gas adsorption with the temperature at 273.15 K in an ice cooling bath and were measured for relative pressure (P/P0) ranging from 0 to 0.03. The density functional theory (DFT) method, Dubinin-Radushkevich (D-R) and Dubinin-Astakhov (D-A) were applied for micropore size, volume, pore surface area, and pore size distribution (PSD). For the mesopores characterization in low pressure (101.3 kPa), liquid N_2 gas adsorption temperature at 77.35 K was calculated for relative pressure (P/P0) ranging from 0 to 0.99, where P is the counterbalance pressure, and P0 is the intensity of the pressure. PSD was analyzed by the BJH method, and Langmuir methods were applied to quantify meso and macropore geometrical shapes and characterizations.

4. Results and discussion

4.1. Coal assay

Table 1 shows the samples were collected from the primary seam,

Table 1
Coal assay results were analyzed on.

Sample No	Depth From - To (m)		Main Coal Seam (m)	M ad	IMC (% db)	VM (% daf)	Ash (% db)	FC (% daf)	C% (% daf)	H% (% daf)	N% (% daf)	S% (% daf)	O% (% daf)	Ro %
SPT-01	268.33	274.83	6.5	24.53	6.57	30.13	8.39	43.1	62.3	5.76	0.48	0.72	39.89	0.4
SPT-14	192.72	198.97	6.25	42.08	7.07	13.68	13.07	37.92	66.84	6.27	0.44	1.44	40.32	0.39
B34	170.55	180.55	10	29.7	7.15	26.76	16.02	37.88	66.11	6.34	0.52	1.13	44.98	0.37
LPT-04	245.2	260.54	15.34	20.94	7.06	37.42	9.31	39.49	63.42	6.01	0.62	0.83	39.38	0.42
LPT-05	221	224	3	22.64	6.43	35.02	12.02	39.25	58.1	5.51	0.57	3.69	45.8	0.38
BMS-02	342.54	344.54	2	13.46	6.75	42.22	11.74	42.53	55.36	5.27	0.51	3.23	48.94	0.4
BMS-04	381.47	382.57	1.1	21.61	6.17	38.37	13.99	36.51	58.48	6.13	0.57	0.24	50.84	0.43
Mean				24.99	6.74	31.94	12.08	39.53	61.52	5.9	0.53	1.61	44.31	0.4

(ADL) air dry loss; (IMC), inherent moisture content; (db), dry basis; (daf) dry, ash-free basis; (VM), volatile matter; (FC), fixed carbon; (Ro%), vitrinite reflectance; (N), nitrogen; (C), carbon; (H), hydrogen; (S), sulfur; (O), oxygen 100- (C + H + S + N), in wt%, daf).

Table 2
Results of the coal-petrological composition of the low-rank coal.

Sample No	Depth From - To (m)		Main Coal Seam (m)	Huminite %							Liptinite %						Inertinite %							
				Telohuminite			Detrohuminite		Gelohuminite															
				Te (A)	Te (B)	Ul (A)	Ul (B)	At	De	Co	Phb	Pg	Cu (S)	Sub	Sp	Re	Ex	Lip	Fu	Sfu	Fg	Sec	Mac	Mic	Int	Total
SPT-01	268.33	274.83	6.50	0	1.9	10.84	19.39	28.71	16.53	3.8	0.38	1.71	0	0.57	0.4	4.94	0	1.33	1.71	3.8	0.76	0	0	0	3.23	100
SPT-14	192.72	198.97	6.25	0	2.02	10.08	18.75	28.23	22.2	1	0	2.62	0.4	0	1.21	5.84	0	1.41	0.6	2.42	1.21	0	0.4	0	1.61	100
B34	170.55	180.55	10	0	1.58	29	23.55	17.05	5.98	4.04	0.53	0.7	0	0	0.88	6.68	0	1.6	0.53	2.29	1.93	0.35	1.05	0	2.28	100
LPT-04	245.2	260.54	15.34	0	5.07	12.19	18.38	20.82	13.32	3.56	0	2.25	0	0	0.75	8.44	0.56	0.93	1.68	7.13	2.62	0	0	0	2.3	100
LPT-05	221	224	3	1.2	4.81	5.41	7.82	22.04	20.45	6.21	0.8	2.81	1.4	0.6	0.8	3.41	1.2	1.8	3.41	4.41	5.41	1	0.6	0	4.41	100
BMS-02	342.54	344.54	2	0	4.31	24.85	31.21	11.91	5.54	1.23	0	0.41	0	0	1.03	6.36	0	0.82	0.62	4.72	3.49	0.82	1.03	0.62	1.03	100
BMS-04	381.47	382.57	1.1	0	0.81	18.22	28.34	14.20	22.26	3.85	0	0.4	0.2	0	0.4	2.42	0	0	2.02	3.04	1.42	0.2	1.21	0	1.01	100
Mean				0.17	2.93	15.8	21.06	20.42	15.18	3.38	0.24	1.56	0.29	0.17	0.78	5.44	0.25	1.12	1.51	3.97	2.41	0.34	0.61	0.1	2.27	100

Te (A), dark gray texinite; Te (B), light gray texinite; Ul (A), dark gray ulminite dark; Ul (B), light gray ulminite; (At), attrinite; (De), densinite; (Co), corpohuminite; (Phb), phlobaphinite; (Pg), porigelinite; Cu (S), small cutinite; Cu (L), large cutinite; (Sub), suberinite; (Sp), sporinite; (Re), resinite; (Ex), exsudatinite; (Lip), liptodetrinite; (Fu), fusinite; (Sfu), semifusinite; (Fg), funginite; (Sec), secrinite; (Mac), macrinite; (Int), inertodetrinite; (mmf), mineral matter free.

which ranged from 1.1 to 15.34 m, and that the thickness of the primary coal seam is greater at the eastern part and decreases towards the western part of the study area. Table 1 also shows the experimental results of proximate, ultimate, and reflectance (Ro%), and the primary seam depth description. Thermal maturity reflecting Ro% ranged from 0.37 to 0.43 (avg. 0.4%), indicating meta-lignite. It was observed that at the primitive stages, pre- or late-biogenic gas was possibly present in the primary coal seam because huminite/vitrinite reflectance is an indicator for CBM generation (Haider et al., 2014). On the air-dry loss basis, the moisture content of coal samples was relatively higher and ranged from 13.46 to 24.53% (avg. 24.99%), and inherent moisture content ranged from 6.17 to 7.15% (avg. 6.74%). The volatile matter (VM) was variable, ranged from 13.68 to 42.22% (avg. 31.94%), whereas ash content of most coal samples were variable and within the range of 8.39–13.99% (avg. 12.08%). The fixed carbon content was similar, varying from 36.51 to 43.10% (avg. 39.51%).

4.2. Coal macerals

The coal macerals group and subgroup classifications (Sýkorová et al., 2005) significantly affect the coal pore structures because they are controlled by chemical and physical changes related to the syndepositional and post-depositional environmental conditions. Table 2 shows low reflectivity in coal particles which indicates that huminite macerals were associated with higher hydrogen content, whereas brighter areas with higher reflectivity indicated inertinite macerals were subjected to higher carbon content (Fig. 3). Huminite content, a dominant maceral, varied from 71.55 to 88.08% (avg. 80.75%). The macerals composition has contributed significantly to the characterization of the pore because a majority of the micro-mesopores are exhibited within the huminite group. Additionally, it is important for micro-mesopore gas to be present within the coal reservoirs because the abundance of huminite has a higher adsorption capacity as compared to other macerals (Beamish et al., 1993; Giffin et al., 2013; Liu et al., 2018; Mastalerz et al., 2008). The macerals subgroups Telohuminite varied from 19.24 to 88.08% (avg. 84.50%), detrohuminite varied from 3.02 to 50.43% (avg. 29.51%), and gelohuminite varied from 3.62 to 12.33% (avg. 7.38%).

Liptinite maceral content was moderately present within the samples, and varied from 3.02 to 10.68% (avg. 8.05%). The dominating maceral within the liptinite group is resinite, which was observed in all the samples. The inertinite macerals group (Fig. 3b and d), which relates to charcoal concentration and a dry environment, demonstrates that a peat mire zone fire occurred during a prolonged time period. Petrographically, the inertinite content exhibited low concentrations that varied from 6.24 to 19.24% (avg. 11.20%). Fusinite is considered to have a higher sorption capacity, but in some cases, fusinite has higher methane adsorption capacity than huminite/vitrinite (Crosdale et al., 1998; Ettinger et al., 1966).

4.3. SEM analysis

SEM analysis is the fundamental parameter for qualitative pore observations within the coal matrix and is visualized at different magnifications (Fig. 4). In low rank coals, primary micropores can be better visualized by SEM at high accelerating voltages (10 kV) and different higher magnifications, while low magnification cannot support the higher zoom (Fig. 4a, c, and e). Low rank coals have higher primary micropores than medium rank coals, which have a sparsity of primary micropores because of deep burial compaction and metamorphism intensity (Cardott and Curtis, 2018; Nie et al., 2015). We observed distinctly different pore structures, pore inhomogeneity trends, and surface characteristics, including elongated smooth and semi-round scummy surfaces of the gas pores (Li et al., 2017a,b; Xin et al., 2019). The examined samples revealed pore openings, cylindrical pores, slit-shaped pore, wedge-shaped pores, and microfractures. Fig. 4 shows the first developed pores observed, and the irregular pore shapes that

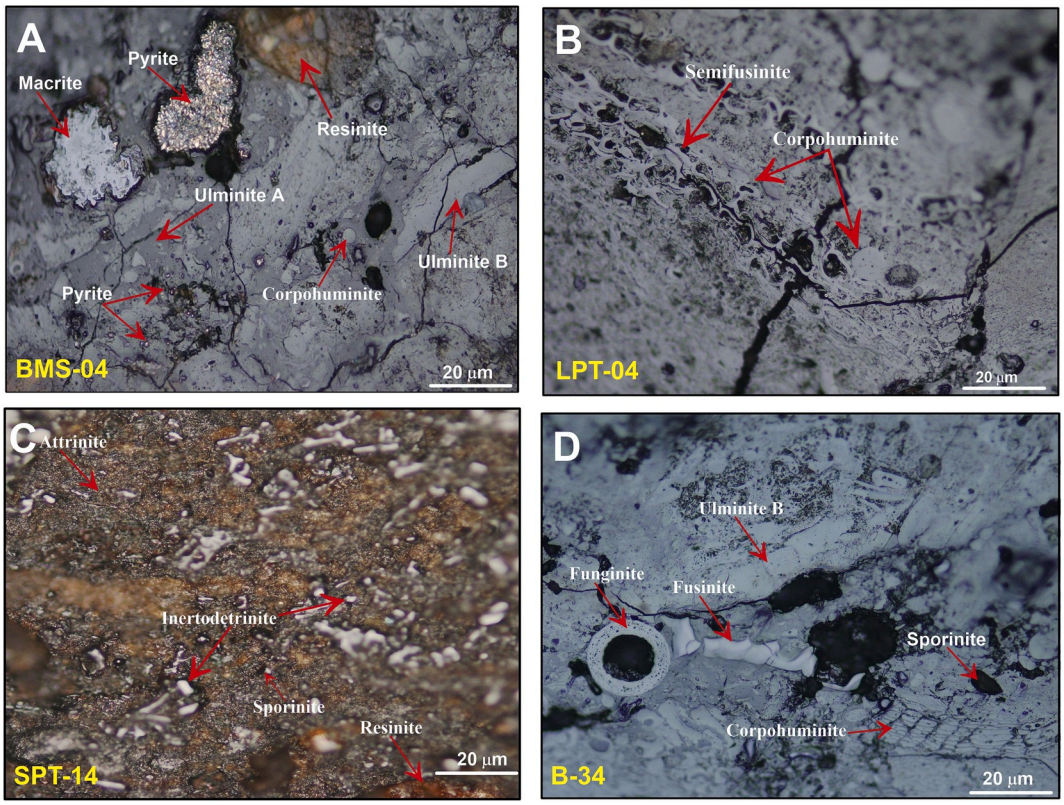

Fig. 3. Photomicrographs of the macerals of the Thar and Badin coalfield areas.

were predominant within these samples. Pore shape dimensions indicate reservoir characteristics and volumetric calculations (Giffin et al., 2013). Fig. 4 focuses on two types of pores in coals: primary pores generally related to plants tissue and thermogenic pores developed by gas desorption process subjected to coalification stages (Chen et al., 2015; Zhang et al., 2010). It can be observed that a large number of interchain pores trending to orderly arranged mainly no filling of mineral matter which suggests late stage gas pore openings. Fig. 4b shows micro-meso gas pores precursor development of larger pores, later connected to microfractures width (<0.1 μm) and length (6 μm>), possibly developed by methane desorption (Chen et al., 2015; Gao et al., 2017; Liu et al., 2015; Xin et al., 2019). Fig. 4b, shows a variety of pore-type configuration affecting accumulation and migration of CBM. Fig. 4c, d, and g show that first developed pores diameters are less than 0.1 μm existing within the larger pores, which were probably a resulting from tissue pore openings within cell lumens (Cardott and Curtis, 2018; Li et al., 2017a,b). The oxidation process caused the first slit-shaped pore developments, and microfracture openings occurred during the coalification process. When low rank coal is under stress, first developed micropores can propagate the open space to generate micro-cracks (Fig. 4c, d and g). Observed cracks are mostly zigzag in shape, their widths range from 0.3 to 0.5 μm and facilitate fluid transportation in the coal zone (Yao et al., 2019).

4.4. CO_2 adsorption isotherms analysis

Fig. 5a shows the geometrical characteristics of the micropore size and surface area at low pressure CO_2 adsorption isotherms and Table 3 shows the analysis data (Brunauer et al., 1940) represents Type I, indicating microporous isotherm solids. Low pressure isotherms exhibited the highest pressure absorbed, and CO_2 revealed the higher amount of organic matter within the coal, unlike in mineral matter. Thar primary coal seam pressure was at 16 cm^3/g in CO_2 adsorbed, whereas Badin was at 11 cm^3/g. It was determined that LPT-04, SPT-01, and SPT-14 had the highest pressure at 17 cm^3/g in the absorbed CO_2, which indicated higher surface area and the highest microporosity. Deitz (1967) reported that OH hydroxyl groups and higher ash yield content within the organic matter of coal sufficiently affected CO_2 absorption, causing a lower micropore surface area. However, it was determined that B-34, BMS-04, and BMS-02 had lower CO_2 adsorption capacity because of low microporosity, indicating higher ash yields for the samples, unlike LPT-04, SPT-01, and SPT-14 with lower ash yields (Table 2).

The D-R transformed isotherms plot leans toward gas molecules being adsorbed at a particular state of energy level on a micropore surface area (m^2/g) of material, and that adsorbed energy level contributed to the linearized form (Fig. 5b). There were uniformly good correlation coefficient results ($R^2 > 0.99$) reflecting uniformity in the micropores surface, and micropore diameter H–K average increased with huminite reflectance (Okolo et al., 2015; Thommes, 2010).

4.5. Micropore size analysis

Fig. 5c and d show that the DFT method was widely applied for micropore size distribution and incremental pore volume following the observed pore diameter range between 0.47 and 1.04 nm that corresponds to higher and smaller particle size peaks. Fig. 5c shows the incremental micropore volume corresponding to varying micropore particle size peaks in three adsorption phases; first phase ranging from 0.47 to 0.68 nm at higher sharp peak values (whereas highest peak values and narrow pore widths observed at LPT-04, SPT-01, and SPT-14 pore ranges). The second phase ranged from The 0.64- to 0.83-nm micropore width has the lowest incremental volume, and peak trend, which is different from the first and third CO_2 adsorbed phases. Widening of the pore width has been observed in the BMS-04, where pore width ranged from 0.73 to 0.82 versus LPT-04 and SPT-14 pore width values of 0.71–0.80 and 0.73 to 0.80, respectively (Fig. 5c). The third phase indicated a 0.83- to 0.92-nm pore width, but samples SPT-01, LPT-05, and SPT-14 had high volume and micropore size widths of

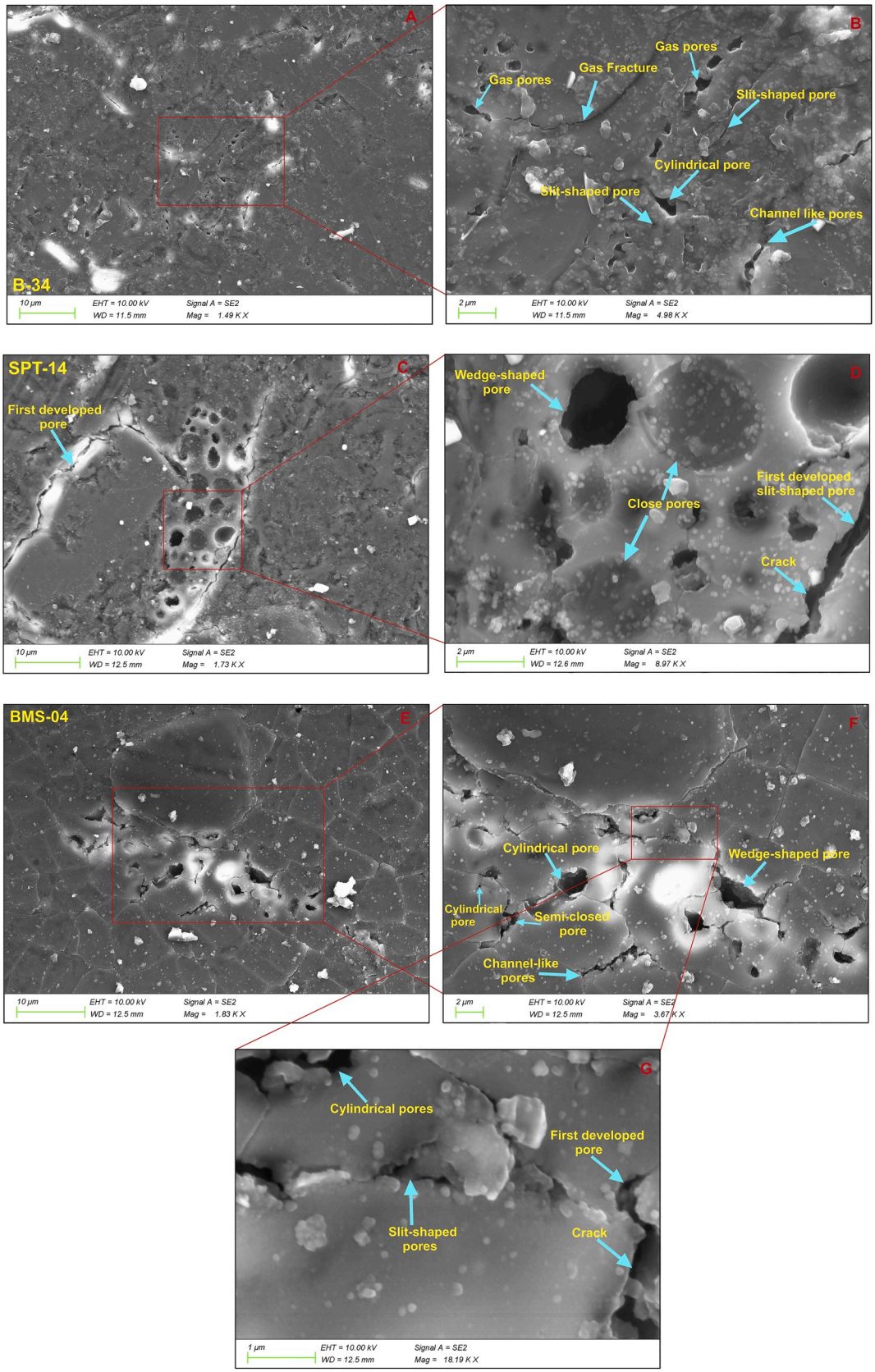

Fig. 4. SEM photographs of a variety of pore structures within the low-rank coal.

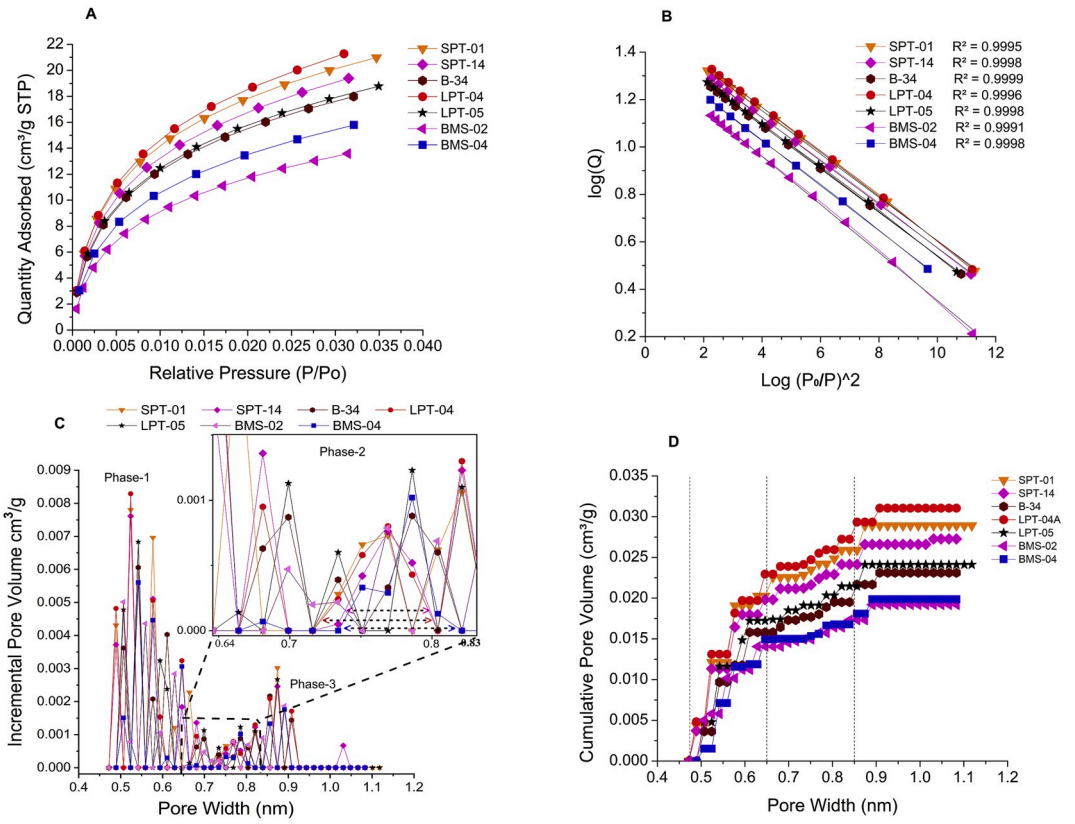

Fig. 5. (A, B) low temperature CO_2, micropore isotherms and transformed isotherm plots; (C, D) the relationship between incremental pore volume and cumulative pore volume.

0.85–0.89 nm. These higher peak trends are different from the second phase micropore width, whereas similar to the first phase.

Additionally, the first and third phase micropore volumes and pore width fractions indicate a micropore tightness tendency to higher incremental pore volumes, unlike the second phase micropore widening or pore diameter that trends toward decreasing pore volume (Fig. 5c). It is assumed that different kind of pores surface areas are present in micropore network and each layer has different gas condensation capacity. The multilayer adsorption capacity mechanism depends upon the different gas pressure which are applied on the micropore surfaces, and are filled as a resultant of gas condensation in the pore region (Gregg et al., 1967; Crosdale et al., 1998). Fig. 4b, c, d, and g show that visualized pore observations exhibit primary/first developed pores into the larger pores. It is generally observed that micropores dominate in the organic material (Mastalerz et al., 2012). Consequently, other factors like clay and minerals can affect the micropores in the coals. The micropore size range and cumulative pore volume results observed at different adsorption gaseous phases substantially increased (Fig. 5d, phase 01 = 0.47–0.64, phase 02 = 0.640.83, and phase 03 = 0.83–11.11), with an increase in micropore pore-size ranges (Hou et al., 2017). However, the incremental and cumulative pore volumes have been observed at different graph trends in incremental pore volumes, exhibiting higher peaks in the first phase. Subsequently, CO_2 sorption gas molecules distort bonding with increasing pore size where the peak values trend from lower to higher and then gradually lower, while cumulative pore volumes remain steady with increasing micropore pore-size ranges. Higher peaks indicate an improved adsorption capacity of the accessible gas molecules in the sample.

4.6. N_2 adsorption isotherms analysis

The low gas pressure N_2 adsorption and desorption isotherms refer to hysteresis loops which attributes the physisorption mechanism and depends on the pore shapes (Anovitz et al., 2015). The results for low rank coals are presented in (Table 3). According to IUPAC classifications by Thommes et al. (2015), the coal samples represent low pressure physiosorption isotherms Type II b suggesting to slit-shaped pores, mostly developed in plate-like particles (Nie et al., 2015; Sing and Chemistry, 1985). There are H4 hysteresis loops (Fig. 6), which are types of isotherms developed on different dimensionally closed micro-meso and macropores pore structures. Fig. 4 shows that SEM exhibits morphologically diverse pore structures; among which the narrow slit-shaped and micro gas fractures hold potential as coalbed gas reservoirs (Fu et al., 2017). Graphical isotherm hysteresis indicates the same adsorption pressure ranges of 0.45–0.9 P/P0, and initial exerted relative pressure developed the monolayer capacity at the range of 0< P/P0 0.45, and subsequently to 0.4 to <0.99 P/P0. The multilayer adsorption capacity increased the hysteresis curves with multilayer adsorption on the micro to macropore wall capillary condensation. Coal sample adsorption capacities suggest that the higher adsorption indicates a higher surface area, which is a good clue for understanding CBM resources (Zhao et al., 2016). Comparing the results with the samples SPT-14, 21.31 cm^3/g STP; BMS-04, 16.67 cm^3/g STP; B-34, 19.46 cm^3/g STP; and LPT-05, 14.25 cm^3/g STP have higher adsorption capacity attributes to higher surface areas. SPT-01, 11.53 cm^3/g STP; LPT-04A, 10.5 cm^3/g STP; and BMS-02, 7.5 cm^3/g STP have lower adsorption and respond to lower surface areas (Table 3). Coal sample hysteresis loops are relatively closer, except that BMS-02 wider hysteresis loop has possible larger particles size exhibits macropores that could resist at the time of equilibration (Mastalerz et al., 2017). Closer hysteresis loop observations are indicating a higher amount of nitrogen sorption exhibit smaller particles, causing complete equilibrium subjected to improved gas transportation within the CBM zone area (Chen et al., 2015; Mastalerz et al., 2017). Low-rank coal specimens exhibited better results of

Table 3
Pore geometrical analytical results were observed on CO_2 and N_2 low pressure adsorption gas; fractal dimension adsorption and desorption Ds values are listed.

Sample No	CO_2				N_2				N_2 Adsorption					N_2 Desorption				
	CO_2 nm	D/R (m^2/g)	D/R (m^3/g)	D/A (cm^3/g)	N_2 nm	BET (m^2/g)	L (m^2/g)	BJH (m^2/g)	BJH (m^3/g)	A_1	D_1	R^2	A_2	D_2	R^2	A_1	D_1	R^2	A_2	D_2	R^2
SPT-01	1.48	150.62	32.97	0.0556	24.75	2.63	3.8	2.69	0.0163	−0.696	2.30	0.96	−0.578	2.42	0.99	−0.631	2.37	0.99	−0.472	2.53	0.99
SPT-14	1.55	141.85	31.05	0.0549	28.75	4.58	6.68	4.83	0.0330	−0.706	2.29	0.96	−0.600	2.4	0.98	−0.667	2.33	0.99	−0.485	2.52	0.99
B-34	1.59	130.96	28.67	0.0521	30.51	3.94	5.77	4.19	0.0302	−0.719	2.28	0.96	−0.604	2.4	0.98	−0.674	2.33	0.99	−0.489	2.51	0.99
LPT-04	1.49	159.23	34.86	0.0593	31.64	2.25	3.25	2.24	0.0179	−0.691	2.31	0.95	−0.615	2.39	0.98	−0.684	2.32	0.99	−0.427	2.57	0.99
LPT-05	1.54	134.31	29.4	0.0516	27.44	3.21	4.63	3.43	0.0221	−0.695	2.31	0.96	−0.591	2.41	0.99	−0.656	2.34	0.99	−0.480	2.52	0.99
BMS-02	1.41	105.86	23.17	0.0372	27.15	1.72	2.45	1.72	0.0116	−0.642	2.36	0.96	−0.568	2.43	0.99	−0.601	2.40	0.99	−0.433	2.57	0.99
BMS-04	1.56	116.95	25.6	0.0455	25.94	3.97	5.72	4.17	0.0258	−0.642	2.36	0.97	−0.581	2.42	0.99	−0.634	2.37	0.99	−0.453	2.55	0.99
Mean	1.52	134.25	29.39	0.0509	28.03	3.19	4.61	3.33	0.0224		2.32	0.96		2.41	0.99		2.35	0.99		2.54	0.99

(nm), micropore size; (D-R m^2/g), micropore surface area; (D-R cm^3/g), monolayer capacity; (D-A cm^3/g), micropore volume; (BET m^2/g), surface area; (L m^2/g), Langmuir surface area; (BJH m^2/g), mesopores area; (BJH cm^3/g), mesopores volume.

specific surface area (1.72–4.58, avg. 3.19 m^2/g), depending upon coal maturity and possibly controlled by the impact of huminite and clay content on the mesopores adsorption process which incorporates to the capillary condensation (Fu et al., 2016; Zhang et al., 2014).

4.7. PSD for mesopore transitional zone

The PSD analysis method revealing a potential quantitative view at the relationship between pore volume and different proportion of pores size in the low rank coal. In this study we focused on transition pores less than 30 nm and are prevalent in the coal, because large proportion of micropores and mesopores internal surface area has sufficient sites for gas adsorption mechanism (Nie et al., 2015). Four graphical representations (Fig. 7) are discussed for this study and PSD, along with differential pore area, pore volume, incremental pore area and pore volume. Based on peak trends the gas adsorption is indicated in the particular pore region and the shape of a different peak at differential pore areas. However, entirely different in an incremental area, overlapping peak trends have also been observed for the particle size and pore diameter in the samples (Fig. 7a and b). Generally, micro-mesopores reside between 1.7 and 11.5 nm within differential pore areas, whereas maximum incremental pore areas reside between 1.8 and 20 nm within transition pore areas. Differential pore areas exhibited higher surface areas and pores within transition zone had higher adsorption pore volume, which is subject to mesopore structural behavior and molecular gas accessibility in mesopores and the majority of the smaller particles. In terms of the B-34 sample that initially overlapped with BMS-04, the BMS-04 and B-34 are essentially the same within the BET (m^2/g) area (Table 3). Compared to the results of specimens exhibiting different peaks within the incremental pore size area at 9 nm, the smaller particles in BMS-04 crossed the SPT-14, where SPT-14 and the LPT05 crossed the B-34 between the transition pore surface areas, which sharply increased to 43 nm. The SPT-14, B-34, BMS-04, and LPT-05 had been observed at the higher surface area (m^2/g), while SPT-01, LPT-04B, and BMS-02 have a lower surface area, compared to the results in (Table 3). The low pressure N_2 adsorption and desorption method close to realistic observation of specific surface area, by comparison, the different pore sizes ranges from 1 to 300 nm which are large proportion widespread in coals (Hou et al., 2017; Mardon et al., 2014; Anovitz et al., 2015). Pore surface area is generally controlled by the PSD between the transition zone (Fu et al., 2017). The following different surface area trends exhibit micro-mesopores within larger pores and SEM observations (Fig. 4). All specimens exhibiting similar graphical trends with pore size ranging between 1.8 and 22.8 nm which indicates maximum differential peak trends within transition pores (Fig. 7e- h). We observed that the differential and incremental graphs of transition pores 17.9 nm, the lower surface area, and pore volume samples had higher peaks trends concerning the higher surface area and pore volume samples. BMS-04 overlapped with SPT-14 the LPT-05 peak overlapped with B-34, and BMS-02 overlapped LPT-04 (Fig. 7b, d, f and h). After 17.9 nm, SPT-14 pore volume supercedes the BMS-04, and 72.5 nm for B-34 pore volume increases compared to BMS-04. Initially BMS-02 pore volume distribution was higher than LPT-04 and SPT-01. In conclusion, the results show that inhomogeneous particle sizes caused the variation in the peaks trends because of smaller pores spheres interconnecting to larger pore spheres. Two phases of gases have been observed which were involved on pore adsorption mechanism: the first phase of gas circulation to the outside of the microsphere surface, and second phase gas circulation in the spaces between micro-mesospheres until the gas molecules reach the outside of the macrospheres (Crosdale et al., 1998). Therefore, the time equilibrium variable at different particle sizes may be constraining the accessible and inaccessible gas molecules in the different pore structures. Coal facies studies show that the huminite maceral group has fine particles size which form early during the carbonization process in mires while semifusinite derived by redox action in mires, produces comparatively larger pores (ICCP, 2001; Liu et al., 2018; Sýkorová et al., 2005).

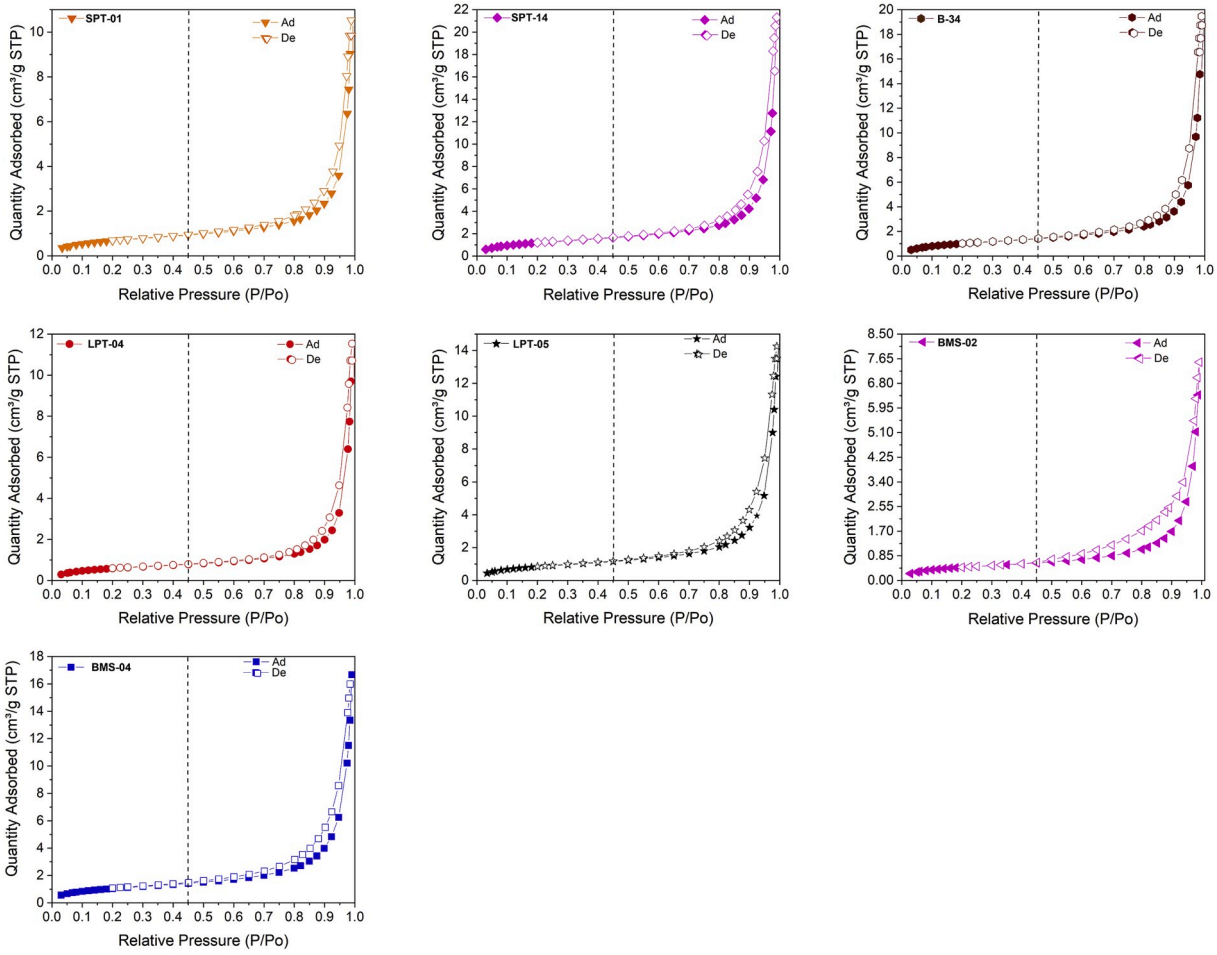

Fig. 6. Low temperature N_2 isotherms plots.

The maximum pore volume (cm^3/g) distribution was identified within the mesopore range of 1.8–20 nm. In addition, coal composition and other factors can affect the pore structure, for example the low volatile coal samples had higher adsorption while high volatile content samples had a lower adsorption process (Tables 2 and 3). Ash content had no direct effect on larger pores, mesopore surface area, and pore volumes (Tables 1 and 3) Likewise, other mineral constituents in the ash content may contribute to higher surface area and pore volume (Mastalerz et al., 2008).

4.8. Fractal dimension of the low-rank coal samples

Mandelbort (1983) developed a mathematical calculation-based model for complex geometrical structures. The multilayer pore distribution is a graphical representation of the existing pore geometrical shape (shapes within the shape connected to the robust heterogeneous architecture of a pore system). For the present study, the Frenkel-Halsey-Hill (FHH) fractal dimension theoretical model was developed (Pfeifer et al., 1989) for multilayer adsorption, and is shown below:

$$\mathrm{In}\left(\frac{V}{V_m}\right) = C + A\left[\mathrm{In}\left(\mathrm{In}\frac{P}{Po}\right)\right] \quad (1)$$

$$A = D - 3 \quad (2)$$

$$A = (D - 3)/3 \quad (3)$$

V represents the volumetric analysis of the sorption gas molecules at the equilibrium pressure P, V_0 is the volume of gas in the monolayer, P is the gas equilibrium pressure, P0 is the gas-saturated pressure, C is the constant value in gas adsorption, A represents the power-law exponent dependent on D and the mechanism of adsorption and C is the constant of gas adsorption. A represents the gas adsorption slope, specified as lnV vs. ln(ln(P0/P), where fractal dimension D linearly depends on line slope A. However, it can be expressed by Equations (2) and (3) and is traditionally applied to quantify the fractal dimension Ds, but both equations are widely used for comparing the different Ds values (Li et al., 2016a,b,c; Pyun and Rhee, 2004; Smith et al., 2005; Yao et al., 2008), which can be directly implied through lnV vs. ln(ln(P0/P) by thermodynamical tension forces directly proportional to the molecular gas condensation on the fractal boundary (Pfeifer and Cole, 1990).

It is important to apply different fractal characteristic study methods on different coal parameters for understanding the coal pore complex structures, particularly those that have a strong link with pore diversities within different coals (Fu et al., 2017; Zhou et al., 2017). In terms of N_2 adsorption and desorption pressure, we examined different fractal dimension analysis methods by means of application to different coal components. Subsequently, other researchers have applied the FHH model on low pressure adsorption Ds values to try to determine coal pore geometrical complexities by using different mathematical equations for porous materials, such as coal pore surface complexity. Following FHH linear plots applied to N_2 adsorption and desorption isotherms, which significantly helped us in the understanding of the pore complexity intrinsically. The FHH straight isotherm line (Fig. 8) results indicate good fittings in linear graphs, with R^2 values for AdDs of 0.98–0.99, and DeDs of 0.96–0.99. Both adsorption and desorption have linear similarity, and thus gas condensation occurs, when the adsorption phase

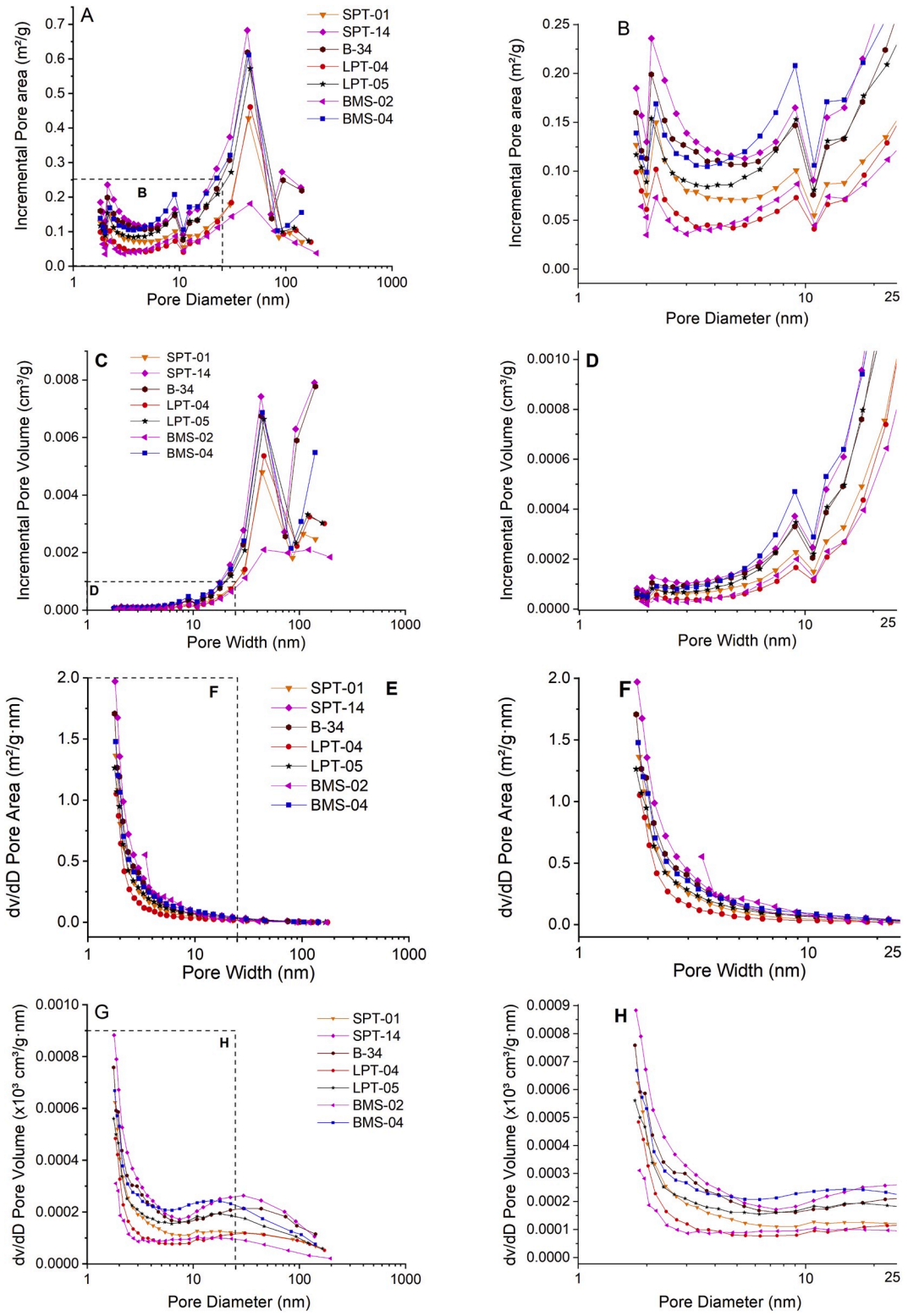

Fig. 7. PSD analysis of differential and incremental pore area peak trends.

occurs. Therefore, these complex pore surface structure attribute changes and retard the absorption. It was determined that during the adsorption stage, $AdDs_1$ averages ranged from 2.29 to 2.36, and $AdDs_2$ ranged from 2.40 to 2.43, unlike the desorption results for $DeDs_1$ at 2.31 to 2.39 and $DeDs_2$ at 2.51 to 2.57. AdDs averaged 2.35 while DeDs averaged 2.44. Correlation was strong between adsorption and desorption, indicating more pores roughness (Figs. 8 and 9) and different relative pressure (e.g., small to large relative pressure increasing in Ds value, representing different pore size rough surfaces) (Zhang et al., 2017b). It was determined that thermodynamic mechanisms dominated among transition pore areas that exhibited pore surface fractal behaviors and heterogonous pore shapes. The Ds value varied from 2 to 3 which suggests that pore surfaces became uneven (Hu et al., 2016; Mandelbrot, 1983; Yang et al., 2016; Yao et al., 2008). The lower Ds value resulted in

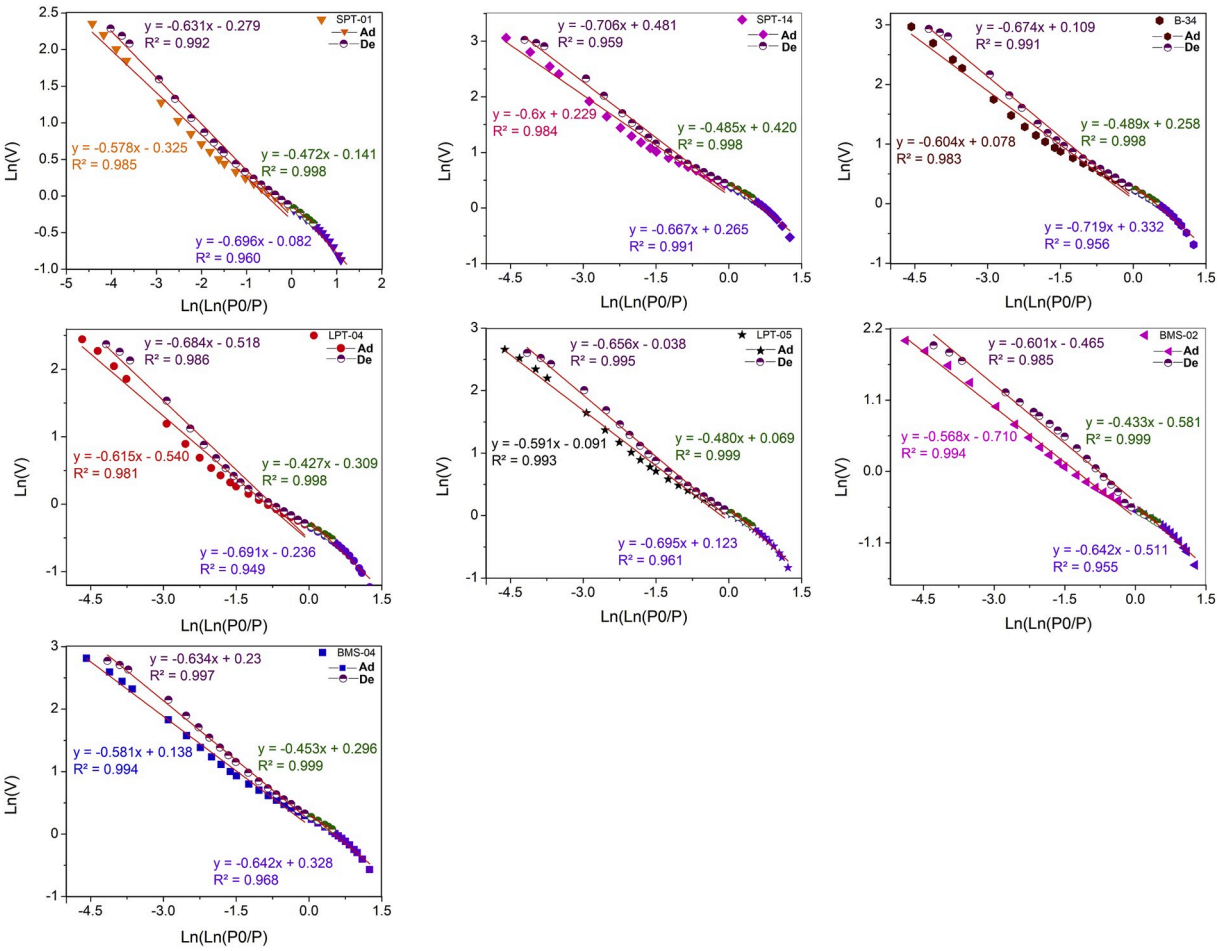

Fig. 8. The relationship between adsorption and desorption Ds values on low-temperature N_2 gas pressure.

more uniform and smooth surfaces, and thus Ds values > 2.4 trend to pore complexities, perhaps good for methane adsorption and indicating the higher surface area fractal dimension; However, in this case, the nature of the porosity is associated within dominating micro and mesopores in the coal (Martin et al., 2011; Sahouli et al., 1996; Sun et al., 2015).

A comparison between PSD and fractal characteristic AdDs relative pressure range P/P0: 0–0.5 suggests 1–5.0 nm where DeDs P/P0 range: 0.5–1 suggests transition pore size structures 5–30 nm, (Zhang et al., 2017b; Zhao et al., 2019). Fig. 9 shows that AdDs values indicate that samples plotted are scattered due to possible variation in pore sizes (Zhang et al., 2014). DeDs samples are show the same trend on the graph and it seems complex pore structures are probably narrow toward widening pore openings in lower gas adsorption, which likely reflects the widening on pore surface development and desorption capacity. Higher sorption capacity on the coal matrix may make it difficult to desorb the gas molecules where there is likely limited access of gases/fluid material (Mahnke and Mögel, 2003; Yao et al., 2008; Zhang et al., 2017b). Coal samples with high semifusinite content have higher DeDs complexity, which may be fall out by different pore spheres, such as macrosphere incorporated with microspheres (Crosdale et al., 1998; Mendhe et al., 2017) (Tables 2 and 3). It is assumed that a higher quantity of small pores is associated with transition pores or macropores. This finding suggests that DeDs value is relatively higher, suggesting a pore complexity rather the AdDs value because the geometrical irregularity of pore shapes can block the high energy level of gas molecule diffusion (Zhang et al., 2017b).

5. Conclusions

In this research, different experimental methods were applied to understand the fundamental geometrical characteristics of pores that influence CBM production and coal formation parameters. Our major conclusions include the following:

1) Maceral observations reveal that high semi fusinite content incorporated the higher DeDs complexity because larger pore spheres consist of micro-mesopore spheres.
2) SEM studies show that irregular and channel pores are connected and there were two types of pore structures. Primary micropores, first developed slit-shaped pores, and gas pores caused the development of larger pores connectedto micro gas fractures, which may possibly be developed by methane desorption.
3) Lower micropore surface area may be determined by higher ash yield content within the organic matter of coal by affecting CO_2 absorption.
4) In this study, micropore size distribution can be better observed by incremental pore volume on different particle size peaks in three adsorption phases. Each adsorption phase has different gas condensation capacity, and this possibly due to the presence of different kind of pores surface areas associated with micropore network.
5) The mesopores distribution analysis on differential and incremental pore areas suggests major graphical intersecting points at transition zones 1.8–22.8 nm, indicating the majority of the micro-mesospheres are present at transition zone, whereas smaller porespheres are interconnected with macrosphere.

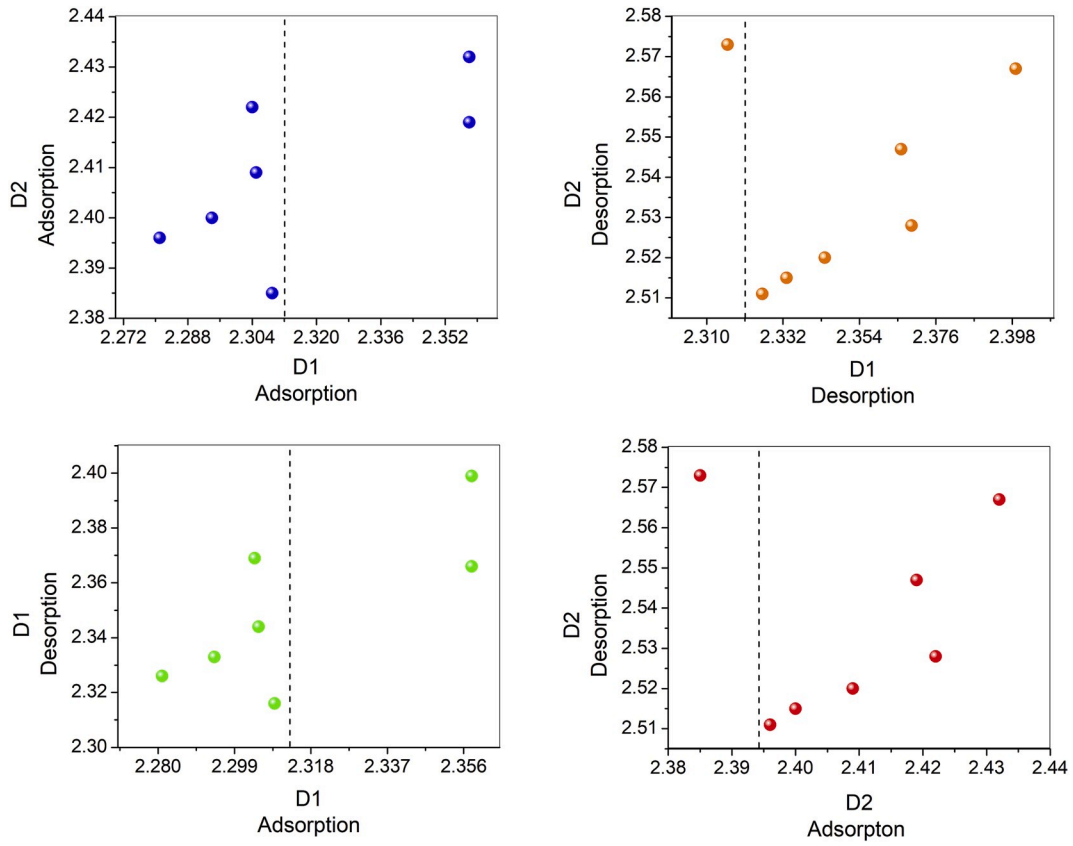

Fig. 9. Fractal characteristic correlations between adsorption and desorption Ds values.

6) For fractal characteristics, four separate Ds value methods were applied to determine the linear correlation relationship, and showed good linearity R^2 values. AdDs average was 2.35, and DeDs average value was 2.44. A higher DeDs value indicates the pore complexities more than pore surface. This indicates that the DeDs value has a strong potential to quantify the pore complexity in the CBM reservoir.

Declaration of competing interest

All authors declare no conflicts of interest.

CRediT authorship contribution statement

Hassan Nasir Mangi: Conceptualization, Formal analysis, Investigation, Methodology, Resources, Software, Writing - original draft. **Yan Detian:** Supervision, Project administration, Funding acquisition. **Nayima Hameed:** Formal analysis, Validation. **Umar Ashraf:** Writing - review & editing, Visualization. **Riaz Hussain Rajper:** Data curation, Resources, Investigation.

Acknowledgements

We are thankful to Geological survey of Pakistan (GSP), Sindh coal authority, Sino Sindh resources Block-I and Under Coal Gasification (UCG), Block-V who provided us chance to obtain the coal core samples for this study. The authors sincerely appreciated Prof. Manoj K Pandit, Dr. Rachel Rawle and two reviewers for their extraordinary support to improve the manuscript. This research was supported by the Natural Science Foundation of China (41690131, 41572327), Natural Science Foundation of Hubei Province (2019CFA028) and the Program of Introducing Talents of Discipline to Universities (No. B14031).

Appendix A. Supplementary data

Supplementary data to this article can be found online at https://doi.org/10.1016/j.jngse.2020.103231.

References

Bale, H.D., Schmidt, P.W., 1984. Small-angle X-ray-scattering investigation of submicroscopic porosity with fractal properties. Phys. Rev. Lett. 53 (6), 596.
Beamish, B., Crosdale, P., Gamson, P., 1993. Characterising the Methane Sorption Behaviour of Banded Coals in the Bowen Basin, Australia.
Boger, C., Marshall, J.S., Pilcher, R.C., 2014. Worldwide coal mine methane and coalbed methane activities. In: Coal Bed Methane. Elsevier, pp. 351–407.
Brunauer, S., Deming, L.S., Deming, W.E., Teller, E., 1940. On a theory of the van der Waals adsorption of gases. J. Am. Chem. Soc. 62 (7), 1723–1732.
Bustin, R., Clarkson, C., 1998. Geological controls on coalbed methane reservoir capacity and gas content. Int. J. Coal Geol. 38 (1–2), 3–26.
Cardott, B.J., Curtis, M.E., 2018. Identification and nanoporosity of macerals in coal by scanning electron microscopy. Int. J. Coal Geol. 190, 205–217.
Chen, R., Qin, Y., Zhang, P., Wang, Y., 2018. Changes in pore structure of coal caused by CS2 treatment and its methane adsorption response. Geofluids 2018. https://doi.org/10.1155/2018/7578967.
Chen, T., Zhou, Z., Han, R., Meng, R., Wang, H., Lu, W., 2015. Adsorption of cadmium by biochar derived from municipal sewage sludge: impact factors and adsorption mechanism. Chemosphere 134, 286–293.
Clarkson, C., Bustin, R., 1999. The effect of pore structure and gas pressure upon the transport properties of coal: a laboratory and modeling study. 1. Isotherms and pore volume distributions. Fuel 78 (11), 1333–1344.
Clarkson, C.R., Freeman, M., He, L., Agamalian, M., Melnichenko, Y., Mastalerz, M., Blach, T., 2012. Characterization of tight gas reservoir pore structure using USANS/SANS and gas adsorption analysis. Fuel 95, 371–385.
Crosdale, P.J., Beamish, B.B., Valix, M., 1998. Coalbed methane sorption related to coal composition. Int. J. Coal Geol. 35 (1–4), 147–158.
Cui, X., Bustin, A., Bustin, R.M., 2009. Measurements of gas permeability and diffusivity of tight reservoir rocks: different approaches and their applications. Geofluids 9 (3), 208–223.
Day, S., Sakurovs, R., Weir, S., 2008. Supercritical gas sorption on moist coals. Int. J. Coal Geol. 74 (3–4), 203–214.
Deitz, V.R., 1967. The adsorption of carbon dioxide on carbon solids. I. Graphite and diamond at 0. degree. J. Phys. Chem. 71 (4), 830–837.

M, Y. Ettinger, I., Eremin, I., Zimakov, B., 1966. Natural factors influencing coal sorption properties. I. Petrography and sorption properties of coals Fuel 45 (4), 267–&.
Fassett, J.E., Durrani, N.A., 1994. Geology and Coal Resources of the Thar Coal Field, Sindh Province, Pakistan, 2331-1258.
Fu, H., Tang, D., Xu, H., Tao, S., Xu, T., Chen, B., Fuels, 2016. Abrupt changes in reservoir properties of low rank coal and its control factors for methane adsorbability. Energy Fuels 30 (3), 2084–2094.
Fu, H., Tang, D., Xu, T., Xu, H., Tao, S., Li, S., Wang, L., 2017. Characteristics of pore structure and fractal dimension of low-rank coal: a case study of Lower Jurassic Xishanyao coal in the southern Junggar Basin, NW China. Fuel 193, 254–264.
Gao, D., Li, M., Wang, B., Hu, B., Liu, J.J.E., 2017. Characteristics of pore structure and fractal dimension of isometamorphic anthracite, 10, 1881.
Giffin, S., Littke, R., Klaver, J., Urai, J., 2013. Application of BIB–SEM technology to characterize macropore morphology in coal. Int. J. Coal Geol. 114, 85–95.
Gregg, S.J., Sing, K.S.W., Salzberg, H.W, 1967. Adsorption surface area and porosity. J. Electrochem. Soc. 114 (11), 279C-279C.
Haider, R., Ghauri, M.A., Jones, E.J., SanFilipo, J.R., 2014. Methane generation potential of Thar lignite samples. Fuel Process. Technol. 126, 309–314.
Hou, S., Wang, X., Wang, X., Yuan, Y., Pan, S., Wang, X., 2017. Pore structure characterization of low volatile bituminous coals with different particle size and tectonic deformation using low pressure gas adsorption. Int. J. Coal Geol. 183, 1–13.
Hu, J., Tang, S., Zhang, S., 2016. Investigation of pore structure and fractal characteristics of the lower silurian Longmaxi shales in western Hunan and Hubei Provinces in China. J. Nat. Gas Sci. Eng. 28, 522–535.
ICCP, 2001. The new inertinite classification (ICCP System 1994), 80, pp. 459–471.
Li, A., Ding, W., He, J., Dai, P., Yin, S., Xie, F., 2016a. Investigation of pore structure and fractal characteristics of organic-rich shale reservoirs: a case study of Lower Cambrian Qiongzhusi formation in Malong block of eastern Yunnan Province, South China. Mar. Petrol. Geol. 70, 46–57.
Li, A., Ding, W., He, J., Dai, P., Yin, S., Xie, F.J.M., Geology, P., 2016b. Investigation of pore structure and fractal characteristics of organic-rich shale reservoirs: a case study of Lower Cambrian Qiongzhusi formation in Malong block of eastern Yunnan Province, South China, 70, 46–57.
Liu, S.-Q., Sang, S.-X., Liu, H.-H., Zhu, Q.-P., 2015. Growth Characteristics and Genetic Types of Pores and Fractures in a High-Rank Coal Reservoir of the Southern Qinshui Basin. Ore Geol. Rev. 64, 140–151.
Li, W., Zhu, Y.-M., Wang, G., Jiang, B., 2016c. Characterization of coalification jumps during high rank coal chemical structure evolution. Fuel 185, 298–304.
Li, Y., Zhang, C., Tang, D., Gan, Q., Niu, X., Wang, K., Shen, R., 2017a. Coal pore size distributions controlled by the coalification process: an experimental study of coals from the Junggar, Ordos and Qinshui basins in China. Fuel 206, 352–363.
Liu, Y., Kang, J., Zhou, F., Fan, Y., Li, H., 2018. Effects of maceral compositions of coal on methane adsorption heat. Geofluids 2018. https://doi.org/10.1155/2018/7596138.
Li, Z., Liu, D., Cai, Y., Ranjith, P., Yao, Y.J.F., 2017b. Multi-scale Quantitative Characterization of 3-D Pore-Fracture Networks in Bituminous and Anthracite Coals Using FIB-SEM Tomography and X-Ray μ-CT, vol. 209, pp. 43–53.
Mahnke, M., Mögel, H., 2003. Fractal analysis of physical adsorption on material surfaces. Colloid. Surface. Physicochem. Eng. Aspect. 216 (1), 215–228.
Mandelbrot, B., 1975. Les Objets Fractals: Forme, Hasard. Dimension. Flammarion, Paris.
Mandelbrot, B.B., 1983. The Fractal Geometry of nature/Revised and Enlarged Edition. WH Freeman and Co., New York, p. 495, 1983.
Mardon, S.M., Eble, C.F., Hower, J.C., Takacs, K., Mastalerz, M., Bustin, R.M., 2014. Organic Petrology, Geochemistry, Gas Content and Gas Composition of Middle Pennsylvanian Age Coal Beds in the Eastern Interior (Illinois) Basin: Implications for CBM Development and Carbon Sequestration. Int. J. Coal Geol. 127, 56–74.
Martin, A., Loh, W.S., Rahman, K.A., Thu, K., Surayawan, B., Alhamid, M.I., Ng, K.C., 2011. Adsorption isotherms of CH4 on activated carbon from Indonesian low grade coal. J. Chem. Eng. Data 56 (3), 361–367.
Mastalerz, M., Drobniak, A., Strąpoć, D., Acosta, W.S., Rupp, J., 2008. Variations in pore characteristics in high volatile bituminous coals: implications for coal bed gas content. Int. J. Coal Geol. 76 (3), 205–216.
Mastalerz, M., Hampton, L., Drobniak, A., Loope, H., 2017. Significance of analytical particle size in low-pressure N 2 and CO 2 adsorption of coal and shale. Int. J. Coal Geol. 178, 122–131.
Mastalerz, M., He, L., Melnichenko, Y.B., Rupp, J.A., 2012. Porosity of coal and shale: insights from gas adsorption and SANS/USANS techniques. Energy Fuels 26 (8), 5109–5120.
Mendhe, V.A., Bannerjee, M., Varma, A.K., Kamble, A.D., Mishra, S., Singh, B.D., 2017. Fractal and pore dispositions of coal seams with significance to coalbed methane plays of East Bokaro, Jharkhand, India. J. Nat. Gas Sci. Eng. 38, 412–433.
Milliken, K.L., Rudnicki, M., Awwiller, D.N., Zhang, T., 2013. Organic matter–hosted pore system, Marcellus formation (Devonian), Pennsylvania. AAPG Bull. 97 (2), 177–200.
Nie, B., Liu, X., Yang, L., Meng, J., Li, X., 2015. Pore structure characterization of different rank coals using gas adsorption and scanning electron microscopy. Fuel 158, 908–917.
Okolo, G.N., Everson, R.C., Neomagus, H.W., Roberts, M.J., Sakurovs, R., 2015. Comparing the porosity and surface areas of coal as measured by gas adsorption, mercury intrusion and SAXS techniques. Fuel 141, 293–304.
Owen, D.D.R., Shouakar-Stash, O., Morgenstern, U., Aravena, R., 2016. Thermodynamic and hydrochemical controls on CH 4 in a coal seam gas and overlying alluvial aquifer: new insights into CH 4 origins. Sci. Rep. 6, 32407.
Pfeifer, P., Cole, M., 1990. Fractals in surface science: scattering and thermodynamics of adsorbed films. II. New J. Chem. 14 (3), 221–232.
Pfeifer, P., Obert, M., Cole, M., 1989. Fractal BET and FHH theories of adsorption: a comparative study. Proc. R. Soc. Lond. A Math. Phys. Sci. 423 (1864), 169–188.
Pyun, S.-I., Rhee, C.-K., 2004. An investigation of fractal characteristics of mesoporous carbon electrodes with various pore structures. Electrochim. Acta 49 (24), 4171–4180.
Qin, Y., Song, Q., Fu, X., 2005. Discussion on reliability for co-mining the coalbed gas and normal petroleum and natural gas: absorptive effect of deep coal reservoir under condition of balanced water. Nat. Gas Geosci. 16 (4), 492–498.
Sahouli, B., Blacher, S., Brouers, F., 1996. Fractal surface analysis by using nitrogen adsorption data: the case of the capillary condensation regime. Langmuir 12 (11), 2872–2874.
SanFilipo, J.R., 2000. A Primer on the Occurrence of Coalbed Methane in Low-Rank Coals, with Special Reference to its Potential Occurrence in Pakistan (2331-1258). Retrieved from.
Siddiqui, F.I., Pathan, A.G., Ünver, B., Tercan, A.E., Hindistan, M.A., Ertunç, G., Kılıoğlu, Y., 2015. Lignite resource estimations and seam modeling of Thar Field, Pakistan. Int. J. Coal Geol. 140, 84–96.
Sing, K.S.J.P., Chemistry, A., 1985. Reporting Physisorption Data for Gas/solid Systems with Special Reference to the Determination of Surface Area and Porosity (Recommendations 1984), vol. 57, pp. 603–619, 4.
Smith, M.J., Edler, K.J., Rigby, S.P., 2005. An experimental study of gas adsorption on fractal surfaces. Langmuir 21 (6), 2281–2292.
Storck, S., Bretinger, H., Maier, W.F., 1998. Characterization of micro-and mesoporous solids by physisorption methods and pore-size analysis. Appl. Catal. Gen. 174 (1–2), 137–146.
Sun, W., Feng, Y., Jiang, C., Chu, W., 2015. Fractal characterization and methane adsorption features of coal particles taken from shallow and deep coalmine layers. Fuel 155, 7–13.
Sýkorová, I., Pickel, W., Christanis, K., Wolf, M., Taylor, G., Flores, D., 2005. Classification of huminite—ICCP system 1994. Int. J. Coal Geol. 62 (1–2), 85–106.
Thommes, M., 2010. Physical adsorption characterization of nanoporous materials. Chem. Ing. Tech. 82 (7), 1059–1073.
Thommes, M., Kaneko, K., Neimark, A.V., Olivier, J.P., Rodriguez-Reinoso, F., Rouquerol, J., Sing, K.S., 2015. Physisorption of gases, with special reference to the evaluation of surface area and pore size distribution (IUPAC Technical Report). Pure Appl. Chem. 87 (9–10), 1051–1069.
Vredenburg, E., 1909a. Introductory note on the stratigraphy of the Ranikot series. Mem. Geol. Surv. India–Palaeontol. Indica 3, 1–19.
Vredenburg, E., 1909b. Note on the Stratigraphy of the Ranikot Series (Retrieved from).
Xin, F., Xu, H., Tang, D., Yang, J., Chen, Y., 2019. Pore structure evolution of low-rank coal in China. Int. J. Coal Geol. 205, 126–139.
Yang, R., He, S., Yi, J., Hu, Q., 2016. Nano-scale pore structure and fractal dimension of organic-rich Wufeng Longmaxi shale from Jiaoshiba area, Sichuan Basin: investigations using FE-SEM, gas adsorption and helium pycnometry. Mar. Petrol. Geol. 70, 27–45.
Yao, Q., Chen, T., Tang, C., Sedighi, M., Wang, S., Huang, Q.J.E.G., 2019. Influence of moisture on crack propagation in coal and its failure modes, 258, 105156.
Yao, Y., Liu, D., Tang, D., Tang, S., Huang, W., 2008. Fractal characterization of adsorption-pores of coals from North China: an investigation on CH4 adsorption capacity of coals. Int. J. Coal Geol. 73 (1), 27–42.
Yu, Q., 1992. Mine Gas Prevention and Control. China University of Mining and Technology Press, Xuzhou, pp. 1–19.
Zhang, R., Liu, S., Bahadur, J., Elsworth, D., Wang, Y., Hu, G., Liang, Y., 2017a. Changes in pore structure of coal caused by coal-to-gas bioconversion. Sci. Rep. 7 (1), 3840.
Zhang, R., Liu, S., Wang, Y., 2017b. Fractal evolution under in situ pressure and sorption conditions for coal and shale. Sci. Rep. 7 (1), 8971.
Zhang, S., Tang, S., Tang, D., Huang, W., Pan, Z., 2014. Determining fractal dimensions of coal pores by FHH model: problems and effects. J. Nat. Gas Sci. Eng. 21, 929–939.
Zhang, S., Tang, S., Tang, D., Pan, Z., Yang, F., 2010. The characteristics of coal reservoir pores and coal facies in Liulin district, Hedong coal field of China. Int. J. Coal Geol. 81 (2), 117–127.
Zhao, J., Tang, D., Qin, Y., Xu, H., 2019. Fractal characterization of pore structure for coal macrolithotypes in the Hancheng area, southeastern Ordos Basin, China. J. Petrol. Sci. Eng. 178, 666677.
Zhao, J., Xu, H., Tang, D., Mathews, J.P., Li, S., Tao, S., 2016. Coal seam porosity and fracture heterogeneity of macrolithotypes in the Hancheng Block, eastern margin, Ordos Basin, China. Int. J. Coal Geol. 159, 18–29.
Zhou, S., Liu, D., Cai, Y., Yao, Y., 2017. Effects of the coalification jump on the petrophysical properties of lignite, subbituminous and high-volatile bituminous coals. Fuel 199, 219–228.